VNU Journal of Science: Mathematics - Physics

Journal homepage: https://js.vnu.edu.vn/MaP

Original Article

Distinctive Effects between Hydrothermal and Ultrasound Synthesized SnO_2 Nanoparticles on Ceramic $Bi_{1.6}Pb_{0.4}Sr_2Ca_2Cu_3O_{10+\delta}$ Superconductor

Pham The An[1], Do Thi Kim Anh[1], Nguyen Duy Thien[1], Vu Hoang Linh[1], Le Hoang Dung[1], Nguyen Khac Man[2], Tran Hai Duc[1,*]

[1]*VNU University of Science, 334 Nguyen Trai, Thanh Xuan, Hanoi, Vietnam*

[2]*International Training Institute for Materials Science, Hanoi University of Science and Technology, 1 Dai Co Viet, Hai Ba Trung, Hanoi, Vietnam*

Received 22 July 2023
Revised 16 September 2023; Accepted 18 March 2024

Abstract: The effect of additions of two series of SnO_2 nanoparticles synthesized using two different methods on crystal structure and superconductivity of $Bi_{1.6}Pb_{0.4}Sr_2Ca_2Cu_3O_{10+\delta}$ (BPSCCO) superconductors was investigated. Two series of spherical SnO_2 nanoparticles were synthesized independently by using ultra-sonication (US-SnO_2) and hydrothermal (HT-SnO_2) methods. Polycrystalline samples of $(Bi_{1.6}Pb_{0.4}Sr_2Ca_2Cu_3O_{10+\delta})_{1-x}(SnO_2)_x$, where x ranged between 0, 0.002 and 0.004, were fabricated by the solid-state reaction method. X-ray diffraction patterns showed a decrease in the volume fraction of the Bi-2223 and an increase in that of the Bi-2212 phases. Scanning electron microscopy images presented the "needle-like blossom" on the surface of the US-SnO_2 doped samples, while the phenomenon was not found on the HT-SnO_2 doped samples. The T_c was decreased extremely with US-SnO_2 doping while slightly HT-SnO_2 nanoparticle-doped samples. The field dependence of J_c, $J_c(B)$, showed the opposite tendencies on two series of samples: $J_c(B)$ was enhanced on the HT-SnO_2 nanoparticle-doped samples, and that was decreased on UT-SnO_2 nanoparticle-doped samples. The application of the Dew-Hughes model to explore the flux pinning mechanism exhibited that the point-like pinning centers were dominant on the HT-SnO_2 doped samples. On US-SnO_2 doped samples, however, the additional pinning center type was not found and could be explained by the observed over-sized SnO_2 nano-needle.

Keywords: BPSCCO, Bi-2223, J_c, SnO_2 nanoparticle, flux pinning.

* Corresponding author.
E-mail address: dhtran@hus.edu.vn

https//doi.org/10.25073/2588-1124/vnumap.4862

1. Introduction

Numerous investigations have been conducted on the $Bi_2Sr_2Ca_{n-1}Cu_nO_{2n+4+\delta}$ (BSCCO) high-temperature superconductor system since its discovery, aiming to enhance its superconducting properties [1–3]. The BSCCO system consists of three distinct superconducting phases, namely Bi-2201 (n = 1), Bi-2212 (n = 2), and Bi-2223 (n = 3), with corresponding critical temperatures (T_c) of 33 K, 80K, and 110 K, respectively [4, 5]. Among these phases, the Bi-2223 phase has been identified as particularly significant for power-related applications. However, the fabrication of this phase has proven to be challenging, requiring precise sintering conditions in terms of temperature and duration. Previous studies have proposed that partial substitution of Pb at the Bi site within the crystal structure could lower the sintering temperature and time. It has been suggested that the presence of Ca_2PbO_4 facilitates the formation and stabilization of the Bi-2223 phase [6]. Several studies have demonstrated that an optimal Bi:Pb ratio of 1.6:0.4 is required for the formation of the Bi-2223 phase [7]. The Bi-Pb-Sr-Ca-Cu-O (BPSCCO) ceramic superconductor has faced challenges related to flux pinning and the enhancement of critical current density (J_c). To address these issues, researchers have explored various techniques and strategies to create artificial pinning centers [2, 3, 8, 9]. In recent studies, the incorporation of nanoparticles into BPSCCO has been investigated as a means to improve J_c and enhance flux pinning capabilities. Various types of nanoparticles, including Al_2O_3, Cr_2O_3, Fe_3O_4, and TiO_2 nanoparticles, have been employed for this purpose [10-13]. Semiconducting nanoparticles have also gained significant attention due to their favorable properties, including high stability, ease of manufacturing, and low toxicity [14, 15].

In this work, we focussed on investigating the effects of additions of two series of SnO_2 nanoparticles synthesized using two different methods on crystal structure and superconductivity of $Bi_{1.6}Pb_{0.4}Sr_2Ca_2Cu_3O_{10+\delta}$ (BPSCCO) superconductors. The ultra-sonication (US-SnO_2) and hydrothermal (HT-SnO_2) methods offer distinct advantages in terms of control over the size, morphology, and crystalline structure of the nanoparticles [15]. By comparing the subsequent incorporation of the SnO_2 nanoparticles into the (BPSCCO) system, this work aims to elucidate their influence on the crystalline structure, critical properties, and flux pinning mechanism of the superconductor. Preliminary results indicated that the two different fabrication methods yield SnO_2 nanoparticles with distinct morphologies and crystal structures, which in turn influence their interaction with the BPSCCO superconductor. Understanding the underlying mechanisms behind these observed effects is crucial for tailoring the synthesis and addition strategies of SnO_2 nanoparticles in the Bi-Pb-Sr-Ca-Cu-O system. Furthermore, these findings provide valuable insights into optimizing the superconducting performances of the material, which are crucial for practical applications.

2. Experiment

2.1. Preparations of Two Series of SnO_2 Nanoparticles

In this work, SnO_2 nanoparticles were chosen for doping in the BSCCO system. They were prepared via two different methods: the ultrasonic and the hydrothermal methods those are noted as US-SnO_2 and HT-SnO_2, respectively.

The precursor of the US-SnO_2 nanoparticles was $SnCl_2.5H_2O$ and dissolved in distilled water. The NH_4O_4 25% solution was added till the pH of the mixture reached 9 with ultrasonic stirring for 3 hours. After a day, the precipitate was sintered at 400 ^oC for 2 hours.

The HT-SnO_2 was prepared with $ZnSO_4.7H_2O$ and $SnCl_4.5H_2O$ mixed with the distilled water with ultrasonic stirring. After that, the polyvinylpyrrolidone and NaOH solution was added separately to

adjust ~ pH12.2. The mixture of solution was hydrothermally sintered at 200 ºC for 12 hours. The solvent was removed by centrifugation. Finally, the powder was dried for 24 hours.

2.2. Fabrication of $Bi_{1.6}Pb_{0.4}Sr_2Ca_2Cu_3O_{10+\delta}$ Ceramics

The $Bi_{1.6}Pb_{0.4}Sr_2Ca_2Cu_3O_{10+\delta}$ ceramic samples doped with SnO_2 nanoparticles were fabricated by the conventional solid-reaction method. The 99.9% purity precursors of Bi_2O_3, PbO, $SrCO_3$, $CaCO_3$, and CuO were prepared with the stoichiometric ratio of the samples, then thoroughly mixed and ground. The ground mixture was pressed into pellets and calcinated in the air in four stages. Each stage was sintered for 48 hours at 670 °C, 750 °C, 800 °C and 820 °C with the grinding–pressing intermediate process. After that, the superconductor powder was mixed with US-SnO_2 and HT-SnO_2 separately for 0.002 g and 0.004 g for each 1 g of sample. The pure sample was noted as S0, US-SnO_2 doped samples were noted as US2 and US4, and the HT-SnO_2 doped samples were noted as HS2 and HS4, respectively.

The crystalline structure of the samples was investigated using the X-ray diffraction technique with Bruker D8 Advance. The surface morphology of the samples was examined by using scanning electron microscopy with Nova NanoSEM 450. The T_c of the samples was investigated via the temperature dependence of electrical resistivity measurement performed by the four-probe method. The J_c of the samples was calculated via the Bean model from the magnetization curves measured by Quantum Design PPMS EverCool II at 65 K.

3. Results and Discussion

3.1. Crystal Structure

The X-ray diffraction (XRD) analysis of the fabricated samples is presented in Figure 1. The majority of the indexed peaks in the samples corresponded to the Bi-2223 (high T_c) and Bi-2212 (low T_c) superconducting phases. The labels "H" and "L" in the patterns were assigned to distinguish these peaks. In the pure sample, the Bi-2223 phase was predominantly observed. However, as the concentration of SnO_2 nanoparticles increased, the intensity of the Bi-2223 peaks decreased. Conversely, the SnO_2-doped samples exhibited a higher proportion of the Bi-2212 phase. The computed results are summarized in Table 1, which shows the percentage of Bi-2212 and Bi-2223 phases based on the volume fraction values. It can be observed that the percentage of Bi-2212 increases monotonically, while the percentage of Bi-2223 decreases monotonically with increasing content of SnO_2 nanoparticles, regardless of the type of SnO_2 nanoparticles used.

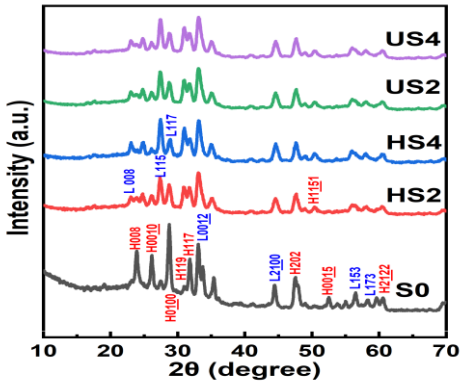

Figure 1. XRD pattern of S0, HT2, HT4, US2, US4 samples.

3.2. Surface Morphology

Surface morphologies of the samples were investigated by SEM images (Figure 2). On the non-doped sample, the crystalline grain is mostly in the plate-like form and composes a dense surface as reported in [5, 16]. Two types of SnO_2 nanoparticle doping conduct different variations on the surface morphology of the samples. Regarding HS2 and HS4 samples, the surface morphology is not changed significantly.

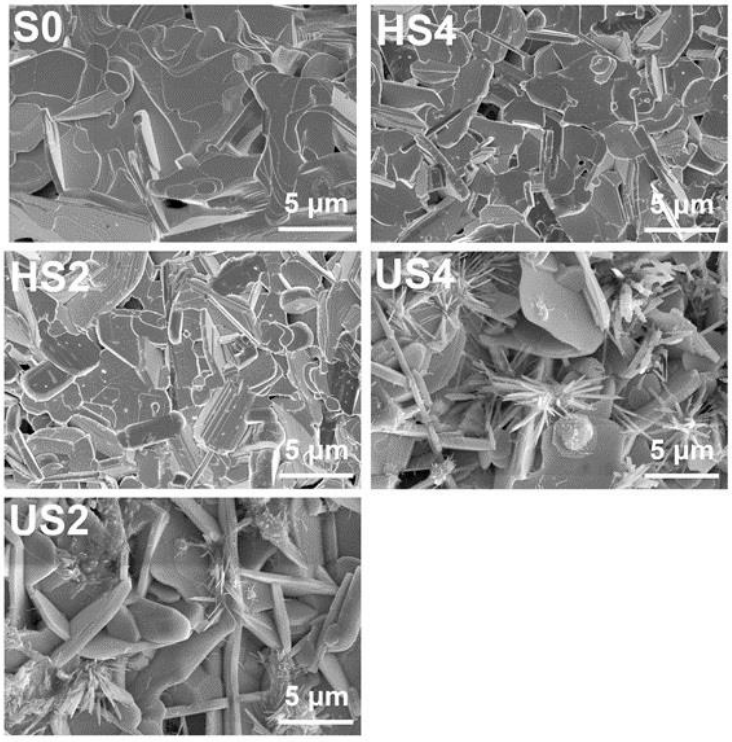

Figure 2. Surface morphology of S0, HT2, HT4, US2, US4 samples.

The grain is gradually misoriented leading to the more frequent appearance of porosity on these samples. However, a needle-like uncorrelated phase appears on the surface of the sample and expands spaciously to the relative with the superconducting grain on the US4 sample. This foreign phase looked like a blooming from a cluster, which was not found on the pure sample. This phenomenon was typically found on SnO_2 nanoparticles [17-20]. Therefore, it can be supposed as the SnO_2 nanoparticle. However, it produces a high misorientation and grain size reduction on superconducting plate-like grain. These needle-like clusters degrade the surface and influence negatively the interconnectivity of the superconducting grains, which would be investigated below. This is a special phenomenon in comparison between the additions of US-SnO_2 and HT-SnO_2 nanoparticles. The different observations between HT-SnO_2 doped and US-SnO_2 doped samples could explain partially the converse decreasing tendency in %Bi-2223, where %Bi-2223 decreases about 10% from HT2 to HT4 sample, but only 3% from US2 to US4 sample. The SnO_2 nanoparticle was undetectable on XRD or SEM results pointing out the good diffusion in the compound. However, the US-SnO_2 nanoparticles were not diffusive as HT-SnO_2 nanoparticles but clumped into needle-like clusters in certain spaces as observed by the sample's morphology.

3.3. Superconducting Properties

To examine the superconductivity of the samples, temperature dependences of resistivity of the samples were measured and shown in Figure 3a. The metallic behavior was found a linear relation at the above transition region on all samples. However, the resistivity of the US2 and US4 samples is significantly higher than the pristine and HS2, HS4 samples. It could be appropriate that the resistivity of the SnO_2 nanoparticle added samples are higher than that of the pure one, and the spacious occupancy of the cluster on the US2 and US4 samples. The T_c of the sample was estimated at the maxima of the first derivatives of the resistivity as a function of temperature relation presented in Figure 3b. As the consideration about the blooming of US-SnO_2 nanoparticles found on SEM images, the T_c of these samples also significantly decreased to 87.74 K on the US2 sample and 86.23 K US4 sample. On the other hand, although the T_c of HS2 and HS4 samples also decreased, with T_c ~ 99.26 K on HS2 and ~96.34 K on HS4 samples, the decrement is significantly smaller. It can be concluded that the blossom of the US-SnO_2 nanoparticle, from spherical to a huge needle-like cluster, affects negatively the formation of the Bi-2223 phase [21].

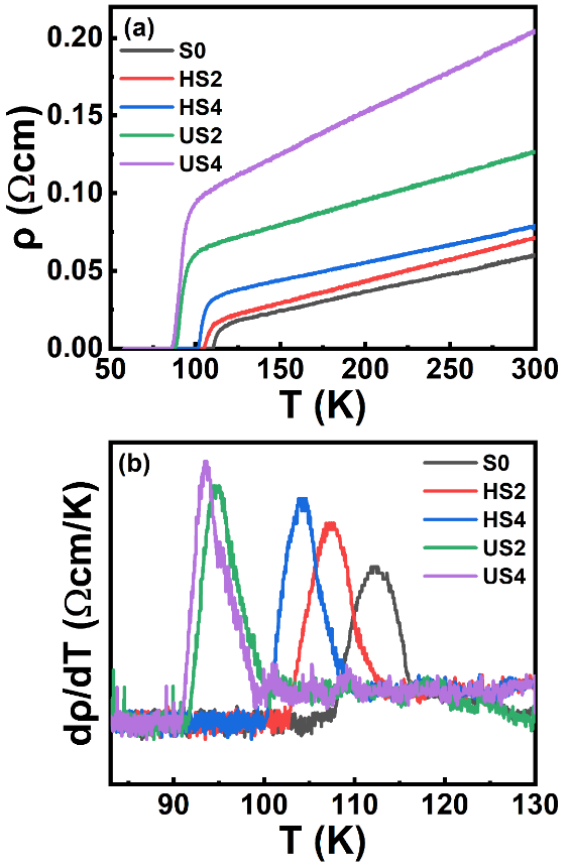

Figure 3. (a) The temperature dependence of resistivity (b) The first derivative of resistivity as a function of temperature of S0, HT2, HT4, US2, US4 samples.

The $J_c(B)$ of the samples at 65 K was calculated by the modified Bean model: $J_c = 20\Delta M/[a(1 - b/3a)]$ and presented in Figure 4 [2, 5, 22]. The contrariant influences were found in the series' two types

of SnO_2 nanoparticle doping. Firstly, the $J_c(B)$ was decreased on the US2 sample, and more significantly on the US4 sample. The results could be forecasted and appropriated with the SEM and *R-T* examinations. The J_c decrement of a superconductor at a defined temperature is an obvious consequence of the T_c decrement. Besides that, the evasion of large needle-like non-superconducting phase and the misorientation can strongly degrade the interconnectivity among the grains. Nevertheless, the J_c is enhanced on both HS2 and HS4 samples, reaching the maximum on the HS2 sample. The J_c of the HS2 sample at B = 0 T reaches 7179 A/cm^2 in comparison with 4124 A/cm^2 of the pristine. It could be explained that the partial SnO_2 nanoparticle could lie on the grain boundary and improve the interconnectivity of the sample, so the self-field J_c was increased. Furthermore, the value of J_c(0.1 T) of HS2 sample was of 4136 A/cm^2 - much larger than that of the pristine in the same field (831 A/cm^2). In this case, it could indicate that the HT-SnO_2 nanoparticle acts as the artificial additional pinning centers. On the HS2 sample, the Bi-2223 phase is dominant, while on the HS4 sample, the %Bi-2223 and %Bi-2212 are not significantly different. However, the Bi-2223 and Bi-2212 are not the same orientation, leading to the degradation of the inter-grain connectivity. Consequently, J_c is not increased effectively in the HS4 sample compared to the HS2 sample.

To investigate the characteristics of the additional flux pinning centers, the Dew-Hughes model was employed using the following function:

$$f_p = Ab^p(1-b)^q$$

where $f_p = F_p/F_{p,max}$ is normalized flux pinning force density, $b = B/B_{irr}$ is the normalized field, Birr is the irreversible field, and A, p, and q are fitting parameters. The q values observed in the samples at all temperatures were found to be approximately 2, indicating core interaction [23]. Consequently, the average values of p for each sample were analyzed to determine the dominant type of pinning centers present. In the undoped sample, the average value of p was determined to be 0.554, indicating the presence of normal core surface pinning centers (p = 0.5) [23]. Previous studies have identified the grain boundaries as the natural pinning centers in BPSCCO polycrystalline superconductors, which aligns with the characteristics of normal core surface pinning centers [23, 24]. On US-SnO_2 doped samples, the value of fitting parameters is not significantly changed, so the dominant pinning center in the samples keeps being the normal core surface pinning center. With the J_c decrement on these samples, the additional pinning center was not found on US-SnO_2 doped samples can be explained that the US-SnO_2 nanoparticles were precipitated into needle-like clusters instead of randomly distributed in the matrix. It was observed that the size of the cluster is about some micrometer, meaning significantly larger than the penetration depth of BSCCO, and becomes oversized of a pinning center for this superconductor. In contrast, with the addition of HT-SnO_2 nanoparticles, the mean values of p showed an increase. The sample with an HT-SnO2 doping of x = 0.002 exhibited the highest p values (approximately p = 0.84), which closely resembled the characteristics of typical normal point pinning (p = 1 and q = 0.2) [23]. The classification of pinning types is influenced by the relative difference between the size of the pinning centers and the values of the penetration depth and coherence length of the superconductor. When the size of the pinning centers is smaller than the penetration depth, core interaction is predicted. On the other hand, if the size of the pinning centers exceeds the coherence length, normal core interaction is expected. In the case of BSCCO, the coherence length (ξ) and penetration depth (λ) are approximately 2.9 nm and 60-1000 nm, respectively [4]. Since the average size of the HT-SnO2 nanoparticles is approximately 11 nm, they are expected to induce normal core interaction. Furthermore, as the size of the SnO2 nanoparticles is smaller than the inter-flux-line distance $d = 1.07(\Phi_0/B)^{1/2}$, it is believed that the HT-SnO2 nanoparticles effectively act as normal point pinning centers [3, 23, 24].

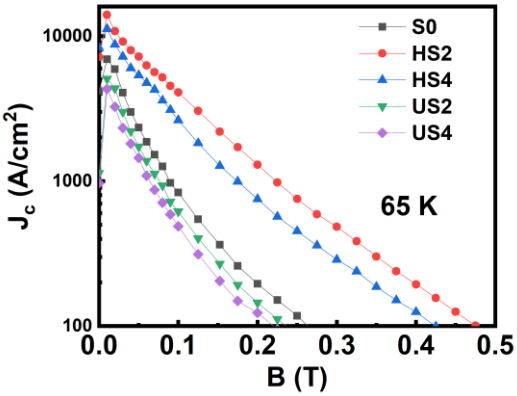

Figure 4. The field dependence of critical current density of S0, HT2, HT4, US2, and US4 samples at 65 K.

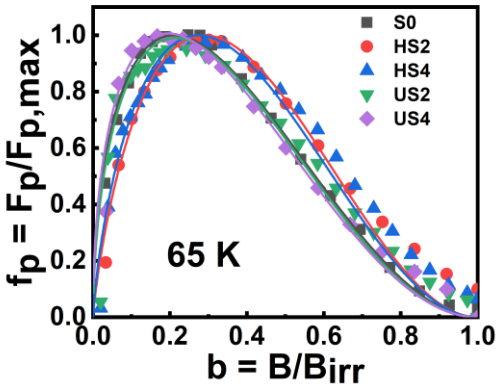

Figure 5. The reduced field dependence of the normalized flux pinning force density of S0, HT2, HT4, US2, and US4 samples.

Table 1. Volume fraction, critical temperature and Dew-Hughes fitting properties of S0, HT2, HT4, US2, and US4 samples

Sample name	%Bi-2223	%Bi-2212	T_c (K)	p	q
S0	67.09	32.91	103.34	0.509	2.013
HT2	64.20	35.80	99.26	0.835	2.011
HT4	54.47	45.53	96.34	0.714	1.999
US2	43.13	56.87	87.74	0.514	2.014
US4	40.88	59.12	86.23	0.508	2.011

4. Conclusion

In summary, this work presents the investigation of the effect of additions of two series of SnO_2 nanoparticles synthesized using two different methods on crystal structure and superconductivity of $Bi_{1.6}Pb_{0.4}Sr_2Ca_2Cu_3O_{10+\delta}$ (BPSCCO) superconductors. Spherical SnO_2 nanoparticles were prepared through ultra-sonication (US-SnO_2) and hydrothermal (HT-SnO_2) methods. Polycrystalline samples with varying SnO_2 doping concentrations (x = 0, 0.002, and 0.004) were fabricated using the solid-state reaction method. The analysis of X-ray diffraction patterns revealed a decrease in the volume fraction of the Bi-2223 phase and an increase in that of the Bi-2212 phase upon SnO_2 adding content. SEM images demonstrated the presence of needle-like blossom structures on the surface of the US-SnO2-added samples, while this phenomenon was not observed in the HT-SnO_2-added samples. In terms of critical properties, the addition of US-SnO_2 nanoparticles resulted in a significant decrease in the critical temperature (T_c), while the HT-SnO_2 doping led to a slight decrease in T_c. The critical current density (J_c) showed an opposite trend, with enhancements of J_c observed in the HT-SnO_2 nanoparticle-added samples. The application of the Dew-Hughes model for analyzing the flux pinning mechanism revealed that the HT-SnO_2 added samples exhibited contributions from point-like pinning centers. On the other hand, the US-SnO_2 added samples did not show the presence of a different type of pinning center, which can be explained by the observed over-sized SnO_2 nano-needle structures.

Acknowledgment

This research was financially supported by University of Science, Vietnam National University, Hanoi under project number TN.22.05.

References

[1] H. Maeda, Y. Tanaka, M. Fukutomi, T. Asano A New High-T_c Oxide Superconductor Without a Rare Earth Element, H. R. Ott, Ten Years Supercond, 1980-1990, Springer, Dordrecht, 1993, pp. 303-304. https://doi.org/10.1007/978-94-011-1622-0_42.

[2] E. S. Nurbaisyatul, H. Azhan, K. Azman, N. Ibrahim, Effect of CeO_2 Nanoparticle on the Structural and Electrical Properties of BSCCO-2223 High Temperature Superconductor, Solid State Phenomena, Vol. 307, 2020, pp. 104-109, https://doi.org/10.4028/www.scientific.net/sSP.307.104.

[3] M. S. Shalaby, M. H. Hamed, N. M. Yousif, H. M. Hashem, The Impact of the Addition of Bi_2Te_3 Nanoparticles on the Structural and the Magnetic Properties of the Bi-2223 High-Tc Superconductor, Ceramics International, Vol. 47, No. 18, 2021, pp. 25236-25248, https://doi.org/10.1016/j.ceramint.2021.05.244.

[4] H. U. Habermeier, Science and Technology of Cuprate-Based High Temperature Superconductor Thin Films, Heterostructures and Superlattices-the First 30 Years (Review Article), Low Temperature Physics, Vol. 42, No. 10, 2016, pp. 840, https://doi.org/10.1063/1.4965889.

[5] B. Özkurt, Improvement of the Critical Current Density in Bi-2223 Ceramics by Sodium-Silver Co-Doping, Journal of Materials Science: Materials in Electronics, Vol. 25, No. 8, 2014, pp. 3295-3300, https://doi.org/10.1007/s10854-014-2017-9.

[6] Ş. Yavuz, Ö. Bilgili, K. Kocabaş, Effects of Superconducting Parameters of SnO_2 Nanoparticles Addition on (Bi, Pb)-2223 Phase, Journal of Materials Science: Materials in Electronics, Vol. 27, No. 5, 2016, pp. 4526-4533, https://doi.org/10.1007/s10854-016-4327-6.

[7] N. H. Mohammed, R. Awad, A. I. A. Aly, I. H. Ibrahim, M. S. Hassan, Optimizing the Preparation Conditions of Bi-2223 Superconducting Phase Using PbO and PbO_2, Materials Sciences and Applications, Vol. 3, No. 4, 2012, pp. 224-233, https://doi.org/10.4236/msa.2012.34033.

[8] S. Zhang, C. Li, Q. Hao, T. Lu, P. Zhang, Influences of Yb Substitution on the Intergrain Connections and Flux Pinning Properties of Bi-2212 Superconductors, Physica C: Superconductivity and Its Applications, Vol. 511, 2015, pp. 26-32, https://doi.org/10.1016/j.physc.2015.02.004.

[9] O. Bilgili, Y. Selamet, K. Kocabaş, Effects of Li Substitution in Bi-2223 Superconductors, Journal of Superconductivity and Novel Magnetism, Vol. 21, No. 8, 2008, pp. 439-449, https://doi.org/10.1007/s10948-008-0374-4.

[10] A. Ghattas, M. Annabi, M. Zouaoui, F. B. Azzouz, M. B. Salem, Flux Pinning by Al-Based Nano Particles Embedded in Polycrystalline (Bi,Pb)-2223 Superconductors, Physica C: Superconductivity and Its Applications, Vol. 468, No. 1, 2008, pp. 31-38, https://doi.org/10.1016/J.PHYSC.2007.10.006.

[11] K. Wei, R. A. Shukor, Superconducting and Transport Properties of (Bi-Pb)-Sr-Ca-Cu-O with Nano-Cr_2O_3 Additions, Journal of Electronic Materials, Vol. 36, No. 12, 2007, pp. 1648-1651, https://doi.org/10.1007/s11664-007-0287-1.

[12] A. T. Pham, D. T. Tran, H. H. Pham, N. H. Nam, L. T. Tai, D. H. Tran, Improvement of Flux Pinning Properties in Fe3O4 Nanoparticle-Doped $Bi_{1.6}Pb_{0.4}Sr_2Ca_2Cu_3O_{10+\delta}$ Superconductors, Materials Letters, Vol. 298, 2021, pp. 130015-1-5, https://doi.org/10.1016/j.matlet.2021.130015.

[13] A. T. Pham, D. T. Tran, L. H. Vu, N. T. T. Chu, N. D. Thien, N. H. Nam, N. T. Binh, L. T. Tai, N. T. M. Hong, N. T. Long, D. H. Tran, Effects of TiO_2 Nanoparticle Addition on the Flux Pinning Properties of the $Bi_{1.6}Pb_{0.4}Sr_2Ca_2Cu_3O_{10+\delta}$ Ceramics, Ceramics International, Vol. 48, No. 14, 2022, pp. 20996-21004, https://doi.org/10.1016/J.CERAMINT.2022.04.093.

[14] S. M. Gupta, M. Tripathi, A Review of TiO_2 Nanoparticles, Chinese Science Bulletin, Vol. 56, No. 16, 2011, pp. 1639-1657, https://doi.org/10.1007/s11434-011-4476-1.

[15] M. A. Dheyab, A. A. Aziz, M. S. Jameel, N. Oladzadabbasabadi, Recent Advances in Synthesis, Modification, and Potential Application of Tin Oxide Nanoparticles, Surfaces and Interfaces, Vol. 28, 2022, pp. 101677, https://doi.org/10.1016/j.surfin.2021.101677.

[16] X. Y. Lu, A. Nagata, K. Watanabe, T. Nojima, K. Sugawara, S. Hanada, S. Kamada, Formation and Texture of Bi-2223 Phase during Sintering in a Temperature Gradient, Physica C, Vol. 412-414, No. Spec. Iss., 2004, pp. 602-606, https://doi.org/10.1016/j.physc.2004.01.080.

[17] Q. Zhao, D. Ju, X. Deng, J. Huang, B. Cao, X. Xu, Morphology-Modulation of SnO_2 Hierarchical Architectures by Zn Doping for Glycol Gas Sensing and Photocatalytic Applications, Scientific Reports, Vol. 5, No. 1, 2015, pp. 1-9, https://doi.org/10.1038/srep07874.

[18] Z. Lu, Z. Zhao, L. Yang, S. Wang, H. Liu, Y. Feng, Y. Zhao, F. Feng, A Simple Method for Synthesis of Highly Efficient Flower-like SnO_2 Photocatalyst Nanocomposites, Journal of Materials Science: Materials in Electronics, Vol. 30, No. 1, 2019, pp. 50-55, https://doi.org/10.1007/S10854-018-0247-Y/METRICS.

[19] I. Fatimah, G. Purwiandono, H. Hidayat, S. Sagadevan, S. A. I. S. M. Ghazali, W. C. Oh, R. A. Doong, Flower-like SnO_2 Nanoparticle Biofabrication Using Pometia Pinnata Leaf Extract and Study on Its Photocatalytic and Antibacterial Activities, Nanomaterials 2021, Vol. 11, No. 11, 2021, pp. 3012, https://doi.org/10.3390/nano11113012.

[20] X. M. Wang, L. Q. Tao, M. Yuan, Z. P. Wang, J. Yu, D. Xie, F. Luo, X. Chen, C. P. Wong, Sea Urchin-like Microstructure Pressure Sensors with an Ultra-Broad Range and High Sensitivity, Nature Communications, Vol. 12, No. 1, 2021, pp. 1-9, https://doi.org/10.1038/s41467-021-21958-y.

[21] G. Yildirim, Beginning Point of Metal to Insulator Transition for Bi-2223 Superconducting Matrix Doped with Eu Nanoparticles, Journal of Alloys and Compounds, Vol. 578, 2013, pp. 526-535, https://doi.org/10.1016/j.jallcom.2013.07.016.

[22] M. S. Shalaby, H. M. Hashem, T. R. Hammad, L. A. Wahab, K. H. Marzouk, S. Soltan, Higher Critical Current Density Achieved in Bi-2223 High-T c Superconductors, Journal of Radiation Research and Applied Sciences, Vol. 9, No. 3, 2016, pp. 345-351, https://doi.org/10.1016/j.jrras.2016.04.001.

[23] D. D. Hughes, Flux Pinning Mechanisms in Type II Superconductors, Philosophical Magazine, Vol. 30, No. 2, 1974, pp. 293-305, https://doi.org/10.1080/14786439808206556.

[24] S. Vinu, P. M. Sarun, R. Shabna, A. Biju, U. Syamaprasad, Improved Microstructure and Flux Pinning Properties of Gd-Substituted (Bi,Pb)-2212 Superconductor Sintered between 846 and 860 °C, Materials Letters, Vol. 62, No. 29, 2008, pp. 4421-4424, https://doi.org/10.1016/j.matlet.2008.07.052.